Available online at www.sciencedirect.com
SCIENCE DIRECT®
ELSEVIER
International Journal of Solids and Structures 42 (2005) 6628–6642
INTERNATIONAL JOURNAL OF SOLIDS and STRUCTURES
www.elsevier.com/locate/ijsolstr

Three-dimensional modeling of the mechanical property of linearly elastic open cell foams

Y.X. Gan, C. Chen *, Y.P. Shen

The State Key Laboratory, School of Civil Engineering and Mechanics, Xi'an Jiaotong University, Xi'an 710049, P.R. China

Received 2 August 2004; received in revised form 2 March 2005
Available online 13 April 2005

Abstract

Three-dimensional Voronoi models are developed to investigate the mechanical behavior of linearly elastic open cell foams. Dependence of the Young's modulus, Poisson's ratio and bulk modulus of the foams on the relative density is evaluated through finite element analysis. Obtained results show that in the low density regime the Young's modulus and bulk modulus of random Voronoi foams can be well represented by those of Kelvin foams, and are sensitive to the geometric imperfections inherent in the microstructure of foams. In contrast, the compressive plateau stress of the foams is less sensitive to the imperfections. Failure surface of the foams subject to multi-axial compression is determined and is found to comply with the maximum compressive principal stress criterion, consistent with available experimental observations on polymer foams. Numerical results also show that elastic buckling of cell edges at microscopic level is the dominant mechanism responsible for the compressive failure of elastic open cell foams.
© 2005 Elsevier Ltd. All rights reserved.

Keywords: Foams; Microstructure; Mechanical properties; Failure surface; Finite element analysis

1. Introduction

Engineered metallic and polymeric foams are increasingly used in applications ranging from ultra-light structural components in air and sea vehicles to energy absorbers in the automobile and packaging industries. Commercially available foams can either have closed-cell or open-cell microstructures, depending on the foaming technology used in the manufacturing processing. Their macroscopic properties are dictated by the solid materials used to produce the foams, and more importantly by the geometrical aspects of the microstructures of the foams, such as the microscopic topology. To facilitate the applications of foams,

* Corresponding author. Tel.: +86 2982663626; fax: +86 2983237910.
E-mail address: cchen@mail.xjtu.edu.cn (C. Chen).

0020-7683/$ - see front matter © 2005 Elsevier Ltd. All rights reserved.
doi:10.1016/j.ijsolstr.2005.03.002

a mature understanding of their properties and their macroscopic responses to external excitation is essential (e.g., Gibson and Ashby, 1997; Ashby et al., 2000).

Since the microstructures of foams are normally of order mm in size and can be easily identified, it is desirable to establish the relationship between the microstructure and the macroscopic mechanical properties of foams. To this end, numerous micromechanics models have been developed (see, for example, Gibson and Ashby, 1997; Banhart, 2001). In general, these models can be categorized into two types. In the first type of modeling, repetitive unit cell models are proposed to provide the homogenized behavior of foams, including two dimensional foam/honeycomb models (Warren and Kraynik, 1987; Gibson and Ashby, 1997; Papka and Kyriakides, 1998a,b; Triantafyllidis and Schraad, 1998; Chen et al., 1999; Gu et al., 2001) and three-dimensional cubic, tetrahedral, and tetrakaidecahedral models (Warren and Kraynik, 1991, 1997; Gibson and Ashby, 1997; Zhu et al., 1997; Gong et al., 2005; Gong and Kyriakides, 2005). Based on the developed unit cell models, the mechanical properties of foams (e.g., the Young's modulus, bulk modulus, multi-axial failure surface, etc.) are evaluated. Although unit cell models have been proven to be useful in understanding some important features of real foams, several drawbacks exist. It is found that they usually over-predict the bulk modulus and hydrostatic yield strength of real foams. To circumvent this drawback, various morphological defects (e.g., non-uniform and wavy cell edges) have to be included (Warren and Kraynik, 1987; Grenestedt, 1998; Simone and Gibson, 1998; Chen et al., 1999). Another problem in unit cell models is that they, in theory, are only applicable to foams with regular and periodic cells whilst real foams always have irregular microstructure.

A second type of micromechanics models, i.e., "super-cell models", has thus been developed in order to give a better representation of the morphological structure of real foams, which usually contains a number of irregular cells. Among them, Voronoi models in conjunction with the finite element method are most widely used. Gibson and her co-workers developed two-dimensional Voronoi models (Silva et al., 1995; Silva and Gibson, 1997). They found that the elastic and plastic uni-axial responses of two-dimensional Voronoi foams to external loading, on average, is not far away from that of periodic regular honeycombs. They also found that removing a few percent of cell edges would lead to sharp decrease in the uni-axial stiffness and strength. Comprehensive analysis of the effects of various morphological defects upon the macroscopic mechanical properties of foams was documented by Chen et al. (1999). By introducing imperfections into the microstructure of foams, Chen et al. predicted an elliptical yield surface for elastoplastic foams under multi-axial loading. The thermal properties of foams have also been analyzed using the Voronoi models (Lu and Chen, 1999). Finite element analysis of three-dimensional Voronoi models is much more computationally challenging. So far, most available studies on three-dimensional Voronoi foams have been limited to investigating their elastic behavior (Kraynik et al., 1997; Shulmeister et al., 1998; Roberts and Garboczi, 2001, 2002; Zhu et al., 2000; Zhu and Windle, 2002). Zhu et al. (2000) found that, at very small values of ρ (e.g., $\rho = 1\%$), the predicted Young's modulus of three-dimensional random Voronoi foams is 50% greater than that of Kelvin foams whilst the bulk modulus of Voronoi foams is about 20% less than that of Kelvin foams. Despite of this discrepancy, the computed uni-axial stress–strain curves of three-dimensional elastic random Voronoi foams, for the compressive engineering strain up to 50%, is quantitatively similar to that of Kelvin foams. Under hydrostatic compression, however, the predicted plateau stress of random Voronoi foams is significantly lower than that of perfect Kelvin foams (Kraynik et al., 1997; Zhu and Windle, 2002).

In this paper, three-dimensional Voronoi models are used to investigate the behavior of elastic open-cell polymer foams. The focus is on the effect of small imperfections upon the simulated macroscopic behavior of foams, and on the failure surface of the foams subject to multi-axial compression. The present paper is organized as follows. In Section 2, three-dimensional Voronoi models used to model the elastic open cell foams are introduced. In Section 3, the foam relative density dependent elastic constants, quantified effect of imperfections on the elastic–plastic properties, and the compressive failure surface of the foams are discussed. A few conclusions on the models and the obtained results are drawn in Section 4.

2. Voronoi models for foams

Finite element models used in this paper to study the mechanical behavior of elastic open cell foams are generated using the technique of Voronoi tessellations (see, for example, Mahin et al., 1980; Okabe et al., 2000), which can be constructed as follows. First, a set of N nuclei are given in a three-dimensional finite space. For each nucleus Q_i ($i = 1,2,\ldots,N$), let cell V_i be the region consisting of all locations in the space which is closer to Q_i than any other nucleus Q_j ($j \neq i$). The space can then be divided into N cells. The boundaries of all cells V_i ($i = 1,2,\ldots,N$) constitute the Voronoi diagram. Note that the Voronoi diagram is unambiguously defined by the pre-given set of nuclei and the common boundary of two adjacent cells V_i and V_j is a perpendicular bisector of the nuclei Q_i and Q_j. In Voronoi tessellations, each cell is separated from others by thin membranes or cell walls. This is more or less similar to the production progress of closed cell foams (Ashby et al., 2000). If the cell walls are removed by chemical treatment or other methods, an open-cell foam structure is obtained, consisting of a network of beams (or cell edges) being interconnected at the vertices. In this study, three-dimensional Voronoi tessellation based "super cell models" are used to study the elastic behavior of open cell foams.

It has been pointed out by Chen et al. (1999) that appropriately applied boundary condition is the key to success for "super cell models" to give representative behavior of real foams. They investigated three different boundary conditions, i.e., prescribed displacement boundary conditions, periodic boundary conditions, and mixed boundary conditions, and concluded that the periodic boundary conditions must be employed in order for "super cell models" to produce faithful results for the ensemble behavior of foams. When prescribed displacement boundary conditions are used, the models usually predict stiffer and stronger response. On the other hand, "super cell models" in conjunction with mixed boundary conditions significantly underestimate the stiffness and strength of foams. It is also noted that when non-periodic boundary conditions are applied, "super cell models" will not keep periodic shape during deformation and the resulting behavior is no longer representative. Similar conclusions were drawn by Zhu et al. (2000) when they studied the elastic constants of three-dimensional Voronoi foams.

The methodology developed by Chen et al. (1999) for two-dimensional "super cell models" is extended to three dimensions. The basic assumption is that the three-dimensional "super cell" Voronoi models of size $L \times L \times L$ adopted in this study is considered to be repetitive blocks of real foams. In other words, the Voronoi models as a whole must be periodic in space. Recall that Voronoi structure is unambiguously determined by the underlying nuclei. The periodicy of Voronoi models is guaranteed if the nuclei are periodically distributed in space. To this end, we first define a cubic box (denoted by A) of size $3L \times 3L \times 3L$ and uniformly divide it into 27 sub-box of the same size $L \times L \times L$, with the central sub-box denoted by B. Randomly distributed nuclei are then generated in the Sub-box B. It should be emphasized that a subsequent nucleus is accepted into Sub-box B only when its distance to any existing nucleus is greater than δ, in order to prevent very small cells in the resulting Voronoi models. The nucleus generation process continues until no more nuclei can be accepted in Sub-box B. The total number of nuclei in Sub-box B depends on the ratio δ/L. The obtained nuclei are then copied into other 26 sub-boxes constituting Box A. All nuclei in Box A are applied to calculate the Voronoi structure using the algorithm developed by Barber et al. (1996). Note from Chen et al. (1999) that the resulting structure is δ-Voronoi structure. By doing this, any super-cell Voronoi model of size $L \times L \times L$ cut from inside the Voronoi structure and not too close to the outer boundary of Box A is periodic in space. As a result, for any boundary node Q of the obtained super cell Voronoi model, there must exist a boundary node Q' at the opposite boundary of the model, with

$$x_i^{Q'} = x_i^Q, \quad x_j^{Q'} = x_j^Q, \quad x_k^{Q'} = x_k^Q \pm L \tag{1}$$

where $i \neq j \neq k$, and x_m^Q and $x_m^{Q'}$ ($m = i,j,k$) are the coordinates of Q and Q', respectively. The relationship between the Voronoi structure in Box A and a resulting *periodic* super-cell model can be better illustrated in the case of two dimensional, by noting that the two-dimensional sizes of Box A and the *periodic* super cell

model are $3L \times 3L$ and $L \times L$, respectively (see Fig. 1a). A typical periodic super cell model for three-dimensional open cell Voronoi foams is shown in Fig. 1b.

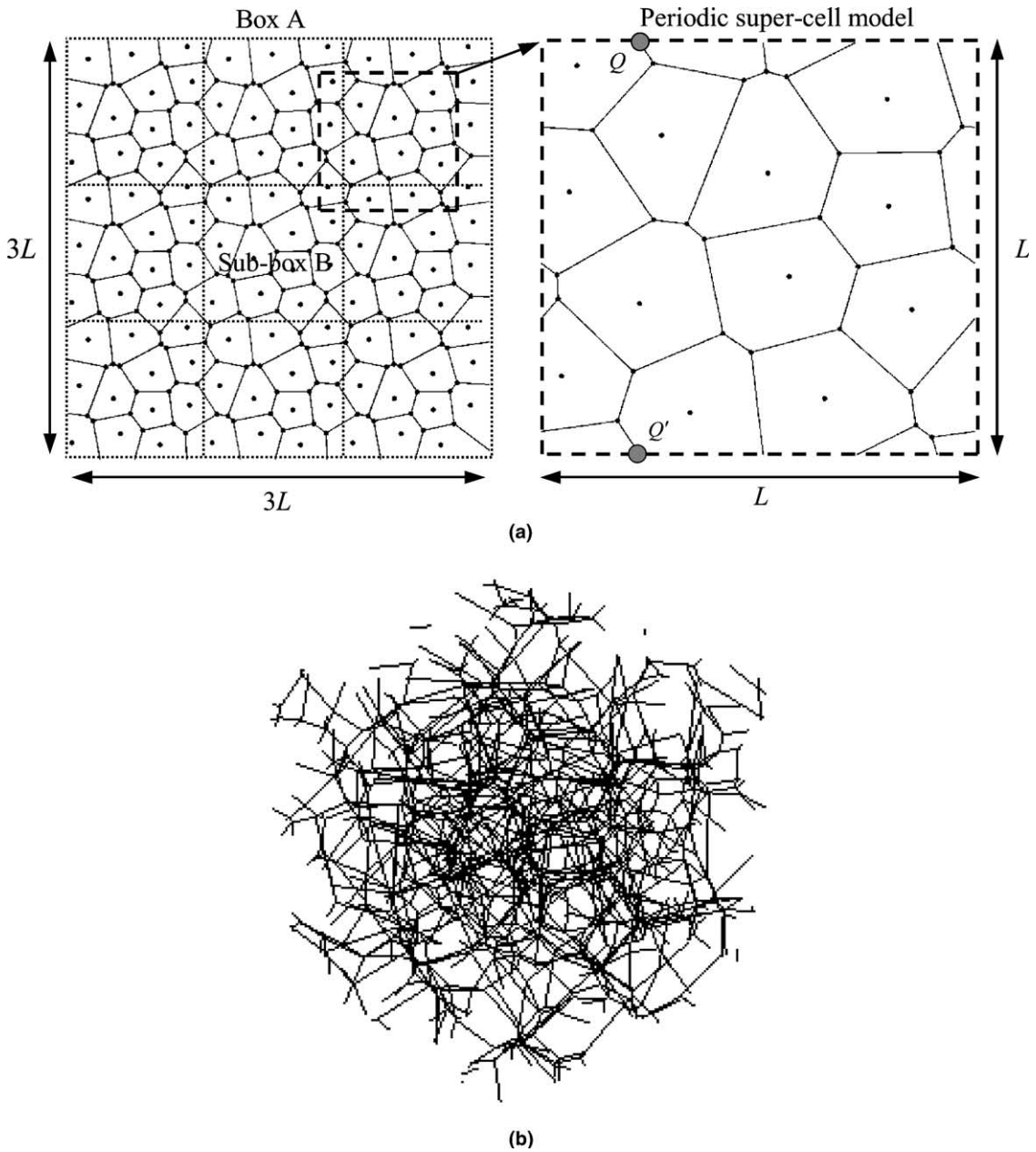

Fig. 1. (a) A two-dimensional drawing showing the relationship between a Voronoi structure in Box A and the derived periodic super cell model. Dark dots refer to the nuclei and vertices of the Voronoi structure. Box A is divided into nine sub-boxes, with the central one denoted by Sub-box B. Nuclei are first generated in Sub-box B and then copied into other sub-boxes. A pair of associated boundary nodes Q and Q' of the periodic model is also marked. (b) A typical three-dimensional Voronoi foam model comprising $5 \times 5 \times 5$ cells.

Periodic boundary conditions can then be applied to the boundary nodes of the resulting periodic Voronoi super cell model through,

$$u_i^{Q'} - u_i^{Q} = \varepsilon_{ij}(x_j^{Q'} - x_j^{Q}), \quad \theta_i^{Q'} - \theta_i^{Q} = 0, \quad i,j = 1,2,3 \tag{2}$$

where superscripts Q' and Q denote a pair of associated nodes on the opposite boundaries, u_i and θ_i are the corresponding displacement and rotation components of the boundary nodes, and ε_{ij} is the macroscopic strain for the "super cell". Details of the boundary conditions (2) are referred to Chen et al. (1999). In the following finite element calculations, the macroscopic stress instead of ε_{ij} is prescribed so that uni-axial stressing, hydrostatic loading or proportional loading is applied during the deformation of the foams.

As usual, the foam relative density is defined as the volume fraction of the solid material of foams. In this study all cell edges of the open cell Voronoi foams are assumed to be uniform beams of the same circular cross-section but of varying length. By denoting the radius of beams by r and the total length of all beams by L_{tot}, a *nominal* relative density can defined as

$$\rho_n = \frac{\pi r^2 L_{\text{tot}}}{L^3} \tag{3}$$

Note that, in expression (3) the mass of intersection points of beams (i.e., the vertices in open cell foams) is not properly accounted for. Wang and Cuitino (2000) gave an improved estimate of the relative density for tetrahedron structures, which can be modified to three-dimensional Voronoi structures. If the number of vertices of a Voronoi structure is N_{inner}, the *true* relative density is then given by:

$$\rho = \frac{27\pi r^2(L_{\text{tot}} - 2\sqrt{2}rN_{\text{inner}}) + 46\sqrt{6}N_{\text{inner}}r^3}{27L^3} \tag{4}$$

We found that the nominal relative density (3) is only appropriate in the low relative density regime and deviates significantly from (4) when the relative density is greater than 5%. Since the foam relative density considered in this paper can be up to 10%, Eq. (4) is used in this study. It should be further noted that, in the following calculations, any desirable relative density of a given foam model can be obtained by assigning appropriate value to the cell edge radius r with other geometric parameters in Eq. (4) fixed.

The macroscopic mechanical response of the elastic Voronoi foam to uni-axial and multi-axial compression is simulated by the finite element analysis code ABAQUS (2003). Each cell edge of the foams is modeled by a few to a number of Timoshenko beam elements (i.e., B32 type elements in ABAQUS), the number of which depends on the slenderness ratio of the cell edge. The Timoshenko beam elements are appropriate for both slender and stout beams. The solid material for cell edges is assumed to be elastic with Young's modulus E_s and Poisson's ratio $\nu_s = 0.345$. This particular value of ν_s is typical for elastic polymer foams.

3. Numerical results and discussion

3.1. Sensitivity of model scale

Since the Voronoi models have random structure, numerical results based on a Voronoi model with only very few cells show too much scatter to draw definitive conclusions on the macroscopic properties. On the other hand, if a Voronoi model consists of too many cells the computational cost would be too high. It is thus necessary to have a trade-off between the number of cells involved in the Voronoi models and repeatable results. To this end, four different scales of Voronoi models are considered: M3, M4, M5, and M6 corresponding to Voronoi models with $3\times3\times3$, $4\times4\times4$, $5\times5\times5$, and $6\times6\times6$ cells, respectively. In each model, 10 random Voronoi foam samples based on different sets of random nuclei are generated. The samples are loaded by uni-axial and hydrostatic compression. The corresponding macroscopic elastic constants

Table 1
Finite element calculated elastic constants based on Voronoi foam models with different model scales

	1	2	3	4	5	6	7	8	9	10	Mean	SD
M3												
E/E_s	2.1461	1.9949	2.1751	2.1612	2.0607	2.084	1.8384	1.7624	1.7957	1.8682	1.9887	0.15956
v	0.4326	0.4456	0.4277	0.4357	0.422	0.425	0.4339	0.4352	0.4338	0.4397	0.4331	0.00693
κ/E_s	5.0492	5.2120	5.1423	5.2552	4.7431	5.0014	4.9964	4.9313	5.1595	5.0735	5.0564	0.14999
M4												
E/E_s	1.9061	2.0521	1.9397	2.1033	2.2014	1.9058	2.1414	2.031	2.1945	1.9075	2.0383	0.11922
v	0.4332	0.4232	0.4352	0.4294	0.4267	0.4356	0.4227	0.431	0.4161	0.4392	0.4292	0.00709
κ/E_s	5.026	4.6279	4.8487	4.8674	5.1267	5.026	4.9068	4.9689	4.934	4.9289	4.9261	0.1337
M5												
E/E_s	2.0502	2.1211	1.9689	2.0572	1.9605	1.8442	1.9075	1.8508	1.8074	1.9939	1.9562	0.10328
v	0.4343	0.4251	0.4341	0.4263	0.4409	0.4363	0.4399	0.4358	0.4379	0.4361	0.4347	0.00521
κ/E_s	4.9784	4.7781	4.9811	4.8526	4.8034	4.9098	5.0431	4.7697	4.857	4.8808	4.8854	0.09237
M6												
E/E_s	1.9316	1.9596	1.8954	1.9822	1.9535	1.9049	1.9669	1.7889	1.9316	1.967	1.9282	0.05637
v	0.43	0.4327	0.4355	0.4271	0.4329	0.4369	0.4295	0.4351	0.4301	0.4308	0.4321	0.0031
κ/E_s	4.8034	4.7489	4.8882	4.7277	4.9164	4.6286	4.941	4.826	4.8034	4.8555	4.8139	0.09442

The foam relative density is 5%, the unit of E/E_s and κ/E_s is 10^{-3}.

such as Young's modulus E , Poisson's ratio v, and bulk modulus κ can be derived from the initial slopes of the computed stress–stain curves. Calculated results for the model foams of relative density $\rho = 5\%$ are summarized in Table 1. It is seen from Table 1 that the averaged predictions based on models with only 27 cells (M3) is not far away from those of models M5 with 125 cells. The observed discrepancy between different examples is less than 10%, which is particularly true for the results on Poisson's ratio. We can conclude from Table 1 that Voronoi models with 125 cells are sufficient to produce representative results. In the following, all calculations are based on M5 Voronoi models. Results averaged from five different samples are reported.

3.2. Dependence on the relative density

Using a cubic foam model, Gibson and Ashby (1997) found that the Young's modulus and bulk modulus of open cell foams are proportional to ρ^2 and ρ, respectively, indicating the respective deformation mechanisms of open cell foams under uni-axial and hydrostatic loading are cell edge stretching and bending. This conclusion has been confirmed by others using perfect Kelvin foam model (Warren and Kraynik, 1997; Zhu et al., 1997). In addition, Zhu et al. (2000) have calculated the dependence of elastic constants (i.e., Young's modulus, Poisson's ratio and bulk modulus) of open cell Voronoi foams upon the relative density and showed that the deformation mechanism of Voronoi foams is similar to that of perfect Kelvin foams in the small relative density regime. The dependence of the elastic constants of Voronoi foams on the relative density is considered here. Recall that Voronoi foams of the same morphological structure but different relative densities are obtained by varying the radius of the constituent cell edges of the foams.

The finite element calculated Young's modulus E, Poisson's ratio v, and bulk modulus κ, denoted by symbols, are plotted in Fig. 2 for relative density in the range 1–10%. Curve fitting the numerical results yields

$$E = \frac{E_s \rho^2}{1 + 6\rho} \tag{5}$$

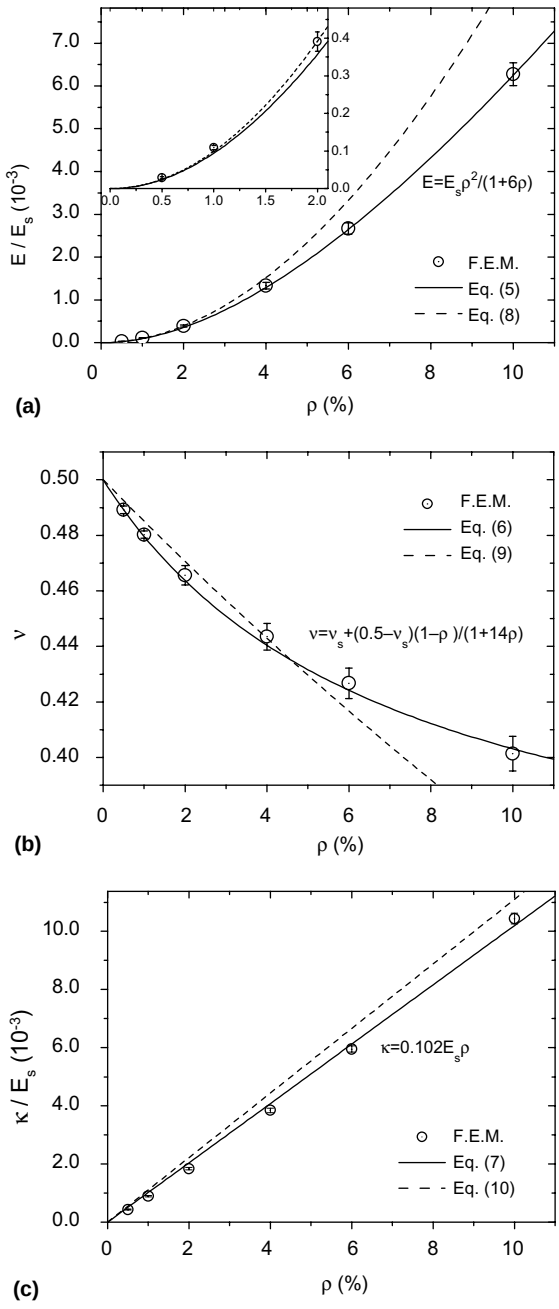

Fig. 2. Relative density dependent elastic constants of open cell Voronoi foams: (a) normalized Young's modulus, (b) Poisson ratio, and (c) normalized bulk modulus. Symbols denote finite element results, and solid and broken lines refer to empirical and analytical results, respectively.

$$v = v_s + (0.5 - v_s)\left(\frac{1-\rho}{1+14\rho}\right) \tag{6}$$

$$\kappa = 0.102 E_s \rho \tag{7}$$

where the special fitting form of Eq. (2) is chosen to match two limiting cases, i.e., $v \to 0.5$ for small ρ and $v = v_s$ for $\rho = 1$. Closed form solutions for the elastic constants of Kelvin foams were obtained by Zhu et al. (1997), as

$$E = \frac{1.009 E_s \rho^2}{1 + 1.514\rho} \tag{8}$$

$$v = 0.5\frac{1 - 1.514\rho}{1 + 1.514\rho} \tag{9}$$

$$\kappa = \frac{E_s \rho}{9} \tag{10}$$

Eqs. (5)–(10) are also included in Fig. 2 for the purpose of comparison, shown as lines. It is seen from Fig. 2 that, in the range of small relative density ($\rho < 2\%$), results (5)–(7) for Voronoi foams are close to those of Kelvin foams (5)–(7): the discrepancy is normally less than 10%. However, Zhu et al. (2000) reported slightly different results for Voronoi foams. Even at very small value of ρ (i.e., $\rho = 1\%$), they found that the predicted Young's modulus of Voronoi foams is 50% greater than that of Kelvin foams whilst the bulk modulus of Voronoi foams is about 20% less than that of Kelvin foams. The underlying reason for the difference between the present results and those by Zhu et al. cannot be readily identified. For larger values of ρ, we note from Fig. 2 that the Young's modulus of Voronoi foams (Eq. (5)) deviates significantly from that of perfect Kelvin foams (Eq. (8)). This could be due to the fact that the present finite element analysis is based on Timoshenko beam elements and can be applied to stout beams, corresponding to foams with moderate values of relative density, while the closed form solutions (8)–(10) are based on Euler–Bernoulli beam theory and are thus only suitable for foams with small ρ. Moreover, it should be noted that the cell edges of real open-cell foams with higher relative density (say above 10%) cannot be simply modeled as uniform beams any more: plateau border effect will prevail in such foams (Warren and Kraynik, 1987; Chen et al., 1999). Therefore, the present finite element analysis may not be applicable to foams of relative density greater than 10% which should be modeled by 3D elements.

3.3. Effect of imperfections

The results shown above are only applicable to ideal random foams without geometrical imperfections. In real foams, however, morphological defects are inevitable and can be introduced either during the manufacturing processing or during in-life service. It has already been found that only a few percent of imperfections could significantly deteriorate some properties of two-dimensional foams (Silva and Gibson, 1997; Chen et al., 1999). Although the defects in real foams can have various morphological features (e.g., wavy cell edges, non-uniform cell edges, cell edge misalignment, broken cell edges etc.), Chen et al. (1999) have showed that imperfection of broken cell edges plays a leading role in degrading the properties of foams. Its effect on the elastic constants of three-dimensional Voronoi foams is discussed in this section, which, once established, is expected to provide a bound to gauge the effect of other types of imperfections on the elastic constants of Voronoi foams.

The broken cell edge imperfection is introduced into Voronoi foams by randomly breaking constituent cell edges of the foams. A damage parameter is defined to quantify the imperfection, i.e., D_{imp} as the ratio of the number of fractured cell edges to the total number of cell edges involved in the model. Subscripts

"imp" refer to imperfections. In Fig. 3, finite element calculated elastic constants for Voronoi foams with imperfections are shown as functions of D_{imp}, denoted by symbols. Three different relative densities

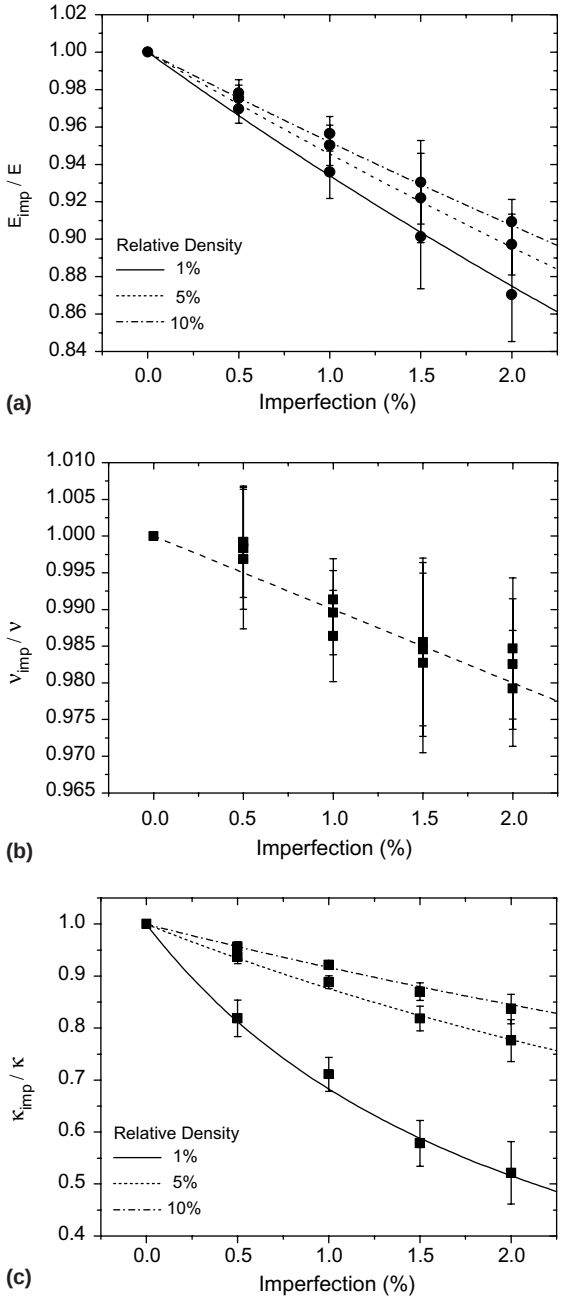

Fig. 3. Effect of imperfections on the elastic constants of open-cell Voronoi foams of density $\rho = 1\%$, 5% and 10%: (a) normalized Young's modulus, (b) normalized Poisson's ratio, and (c) normalized bulk modulus. Symbols denote finite element results, and lines refer to empirical curve fitting results.

$\rho = 1\%$, 5%, and 10% are considered. Results are normalized by the corresponding values of random Voronoi foams without imperfections, for a better illustration of the effect of imperfections. It can be seen from Fig. 3 that except the Poisson's ratio both Young's modulus and bulk modulus are very sensitive to the broken cell edge imperfections. For a given imperfection with D_{imp} being as small as 2%, the Young's modulus can be reduced by about 10%, and the bulk modulus by from 15% to 50%, depending on the relative density of foams. Based on the results shown in Fig. 3, the following empirical expressions can be postulated to account for the effect of broken cell edge imperfections. For the Young's modulus we have

$$\frac{E_{\text{imp}}}{E} = \frac{1 - D_{\text{imp}}}{1 + \alpha_E D_{\text{imp}}} \tag{11}$$

where E is given by Eq. (5) and α_E is a function of the relative density. By fitting Eq. (11) to the finite element calculated results shown in Fig. 3a, we get $\alpha_E = 6$, 4.7, and 4 for $\rho = 1\%$, 5%, and 10%, respectively. The Poisson's ratio of imperfect Voronoi foams when normalized by that of perfect Voronoi foams is given by

$$v_{\text{imp}}/v = 1 - D_{\text{imp}} \tag{12}$$

and the bulk modulus for imperfect Voronoi foams is

$$\frac{\kappa_{\text{imp}}}{\kappa} = \frac{1 - D_{\text{imp}}}{1 + \alpha_\kappa D_{\text{imp}}} \tag{13}$$

Similar to α_E, α_κ in Eq. (13) is evaluated by fitting against the numerical results shown in Fig. 3c, giving α_κ equal to 45, 13, and 8 for $\rho = 1\%$, 5%, and 10%, respectively.

3.4. Failure surface under multi-axial compression

Foams presumably work under compression. Their response to multi-axial compression is of practical importance and is explored in this section. Although the deformation of linearly elastic foams *prior to* elastic buckling failure (the failure mode will be discussed later in the paper) is loading path independent, their stress–strain responses and elastic buckling mode depend on the applied loading. If non-proportional

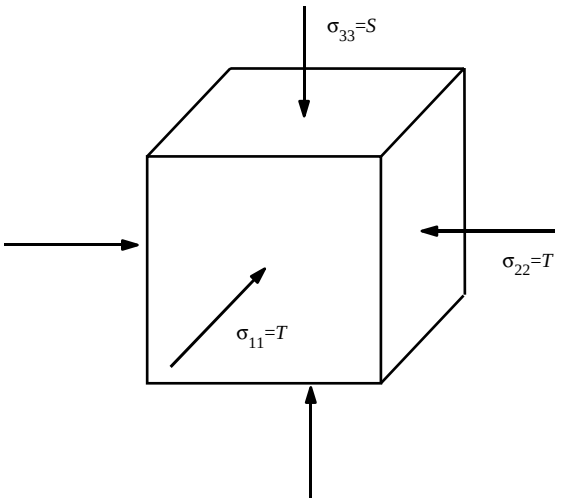

Fig. 4. A sketch of three-dimensional loading imposed upon the open cell Voronoi foams.

loading is considered, simulation of the multi-axial behaviour of the foams would be very complicated. Note that we are only interested in the multi-axial failure surface of the foams. Proportional loadings are sufficient for us to construct the failure surface and are considered in the following. Sketch of foams under three-dimensional loading is shown in Fig. 4, where S and T refers to the axial and lateral loading,

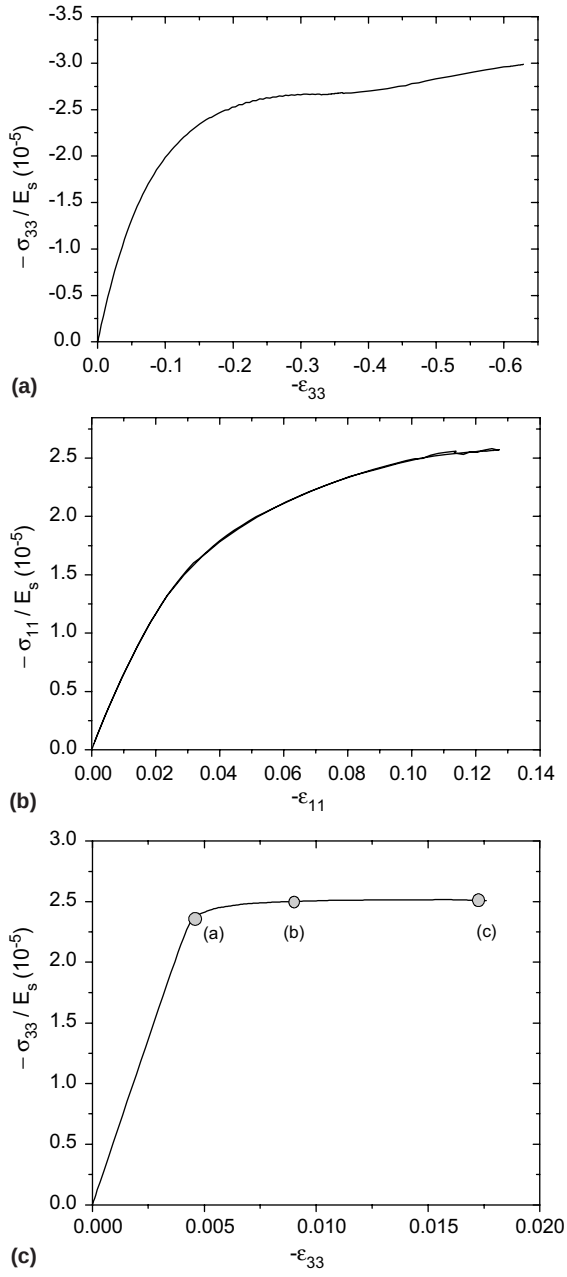

Fig. 5. Typical stress–strain responses of an open-cell Voronoi foam to (a) uni-axial compression (i.e., $T = 0$), (b) equi-biaxial compression (i.e., $S = 0$) and (c) hydrostatic compression (i.e., $S = T$). The relative density of the foam is $\rho = 2\%$.

respectively. Since only proportional loading is considered in this paper, the ratio between S and T is fixed when loading the foams. Failure surface of the foams under multi-axial compression are determined from the predicted stress–strain curves.

Typical finite element simulated true stress–strain curves of a random Voronoi foam without imperfection are shown in Fig. 5 for the case of (a) uni-axial compression, i.e., $T = 0$, (b) equi-biaxial compression, i.e., $S = 0$, and (c) hydrostatic compression, i.e., $S = T$. The relative density is $\rho = 2\%$. All three stress–strain curves in Fig. 5 depict highly non-linear nature and a plateau is present. Since the solid material of the foams considered here is elastic the origin of the non-linearity in the stress–strain curves stems from the large deformation and elastic buckling of cell edges. The later is confirmed by deformed configurations

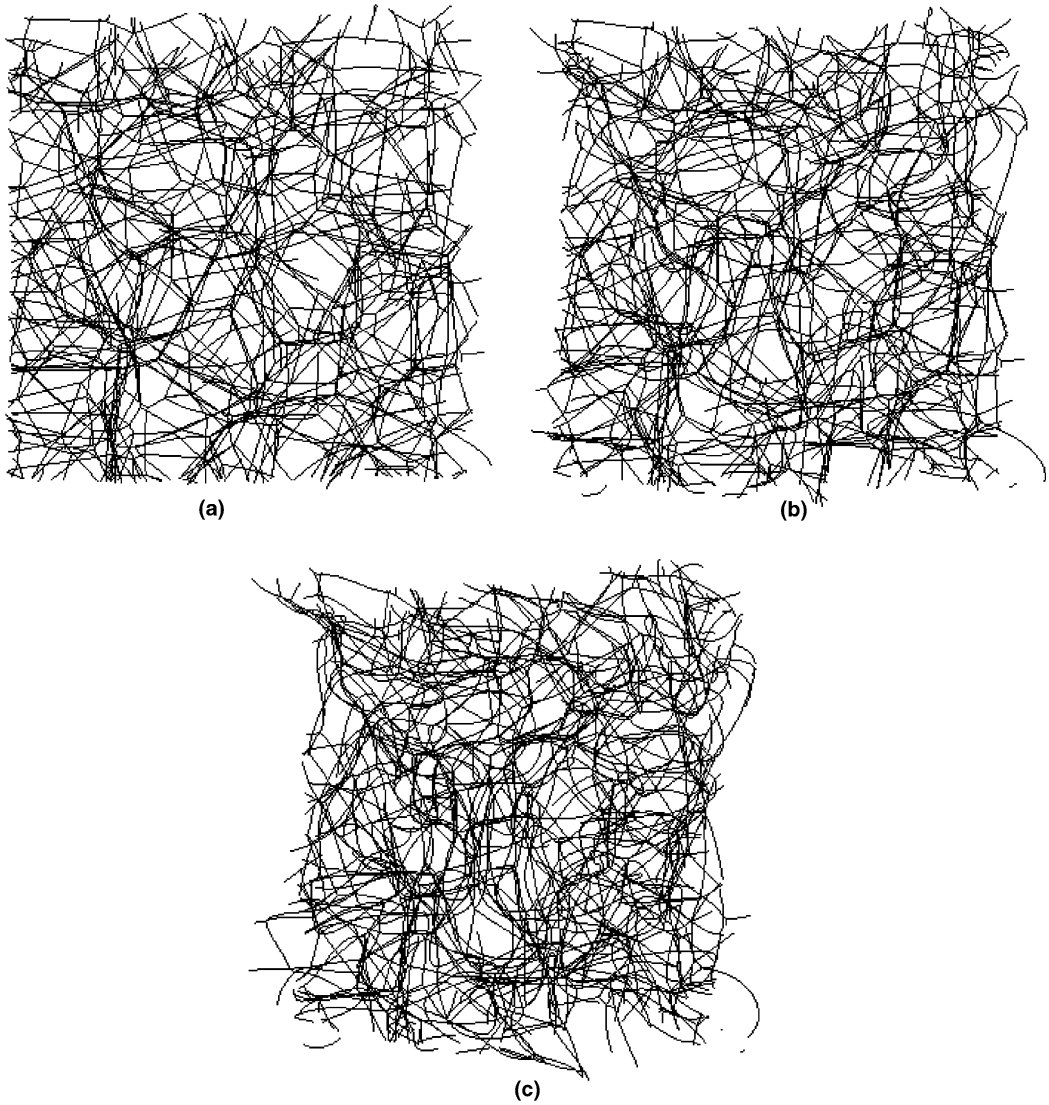

Fig. 6. Deformed shapes of the foam under hydrostatic compression, corresponding to volumetric strain levels labeled in Fig. 5c: (a) $\varepsilon_v = -0.0136$; (b) $\varepsilon_v = -0.0269$; and (c) $\varepsilon_v = -0.0514$. The deformations are magnified by a factor of 5 for a better view.

at three deformation levels indicated on the hydrostatic stress–strain curve in Fig. 5c, see Fig. 6. The volumetric compressive strains corresponding to Figs. 6a–c are 0.0136, 0.0269, and 0.0514, respectively. It is visually clear from Fig. 6c that elastic buckling is responsible for the plateau shown in Fig. 5. Elastic buckling has also been found to be the main mechanism responsible for the plateau stress of the elastic open cell foams under other compressive loadings. Similar finding has also been reported by an experimental study of polymer foams in compression (Deshpande and Fleck, 2001) and by the numerical simulation of elastic open cell foams (Zhu and Windle, 2002).

In order to determine the failure surface, a number of simulations have been carried out for Voronoi foams subject to various proportional loadings. When the stress associated with the plateau of the calculated stress–strain curves (i.e., the plateau stress) is defined as the failure stress of the foams, the failure surface in the $T - S$ space can be constructed. Fig. 7 shows the obtained failure surfaces of the foams. Two densities are considered, with $\rho = 1\%$ and 2%. It is seen from Fig. 7 that the hydrostatic compressive failure stress of elastic open cell Voronoi foams, in magnitude, is comparable to the uni-axial failure stress, and the failure surfaces for both densities comply with the maximum principal compressive stress criterion, consistent with experimental observations by Deshpande and Fleck (2001). Also included in Fig. 7 is the failure surface of a Voronoi foam with relative density $\rho = 2\%$ and imperfection $D_{\text{imp}} = 2\%$. Results in Fig. 7 show that, in general, 2% imperfection reduces the failure stress only by 10% in all loading conditions. Recall that 2% imperfection can reduce the elastic constants by as much as 50% (in bulk modulus). The results in Fig. 7, in conjunction with those in Fig. 3, indicate that the failure stress of open cell foams when compared to elastic constants is less sensitive to imperfections.

Dependence of the hydrostatic compressive failure stress (denoted by σ_{el}) on the relative density has also been explored for open cell Voronoi foams *without* imperfections, see Fig. 8. Curve fitting of the numerical results reveal that σ_{el} is related to the relative density by

$$\sigma_{\text{el}} = 0.0605 E_s \rho^2 \tag{14}$$

It is noted that the power law (14) is not far away from that given by Gibson and Ashby (1997) for the uni-axial buckling stress of cubic open cell foams, that is

$$\sigma_{\text{el}} = 0.05 E_s \rho^2 \tag{15}$$

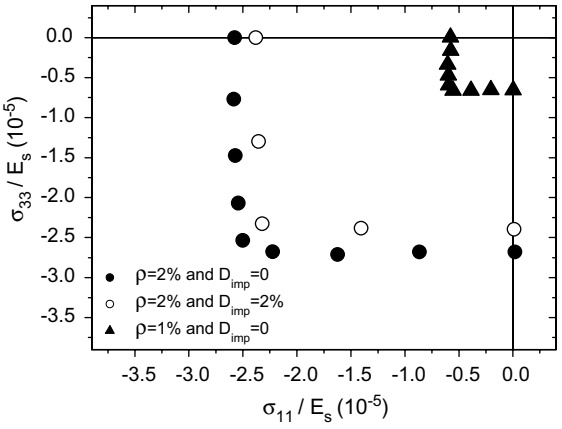

Fig. 7. Failure surfaces of elastic open-cell Voronoi foams under multi-axial compression. Three foams with different relative densities and imperfections are considered.

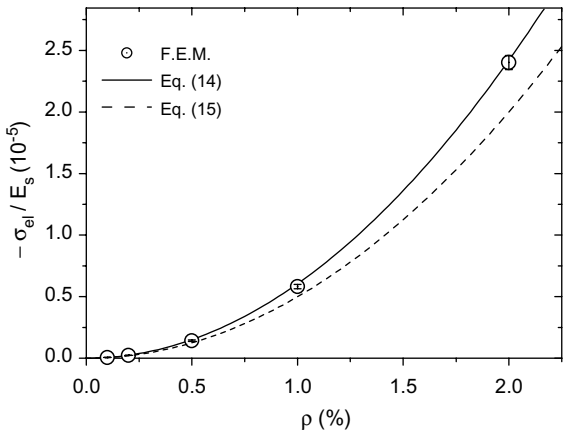

Fig. 8. Dependence of the hydrostatic buckling stress σ_{el} of open-cell Voronoi foams on the relative density. Symbols denote finite element results, and lines refer to empirical results.

4. Conclusions

Three-dimensional random Voronoi models are developed to simulate the macroscopic mechanical behavior of elastic open cell foams under compressive loading. In the small relative density regime, it is found that the elastic constants predicted by random Voronoi foam models are not far away from those by perfect Kelvin foam models. In the high relative density regime, however, Kelvin foam models over-estimate the Young's modulus and bulk modulus of random foams. Obtained results also show that the Young's modulus and bulk modulus of Voronoi foams are very sensitive to imperfections whilst the plateau stress of the foams subject to compression is less sensitive. Systematic numerical simulations have been carried out to investigate the macroscopic failure response of elastic open cell Voronoi foams under multi-axial compression. Micro-buckling of cell edges is identified as the dominant mechanism responsible for the failure of the foams in compression. Compressive failure surfaces of the foams are constructed from the calculated stress–strain curves and are found to comply with the maximum compressive principal stress criterion, which is consistent with available experimental results.

Acknowledgment

The authors are grateful for the financial support by the Natural Science Foundation of China (10302024, 10425210) and the Ministry of Education of China.

References

ABAQUS. Standard User's Manual, Version 6.2, 2003. Hibbitt, Karlsson and Sorensen, Inc., Providence, Rhode Island.

Ashby, M.A., Evans, A.G., Fleck, N.A., Gibson, L.J., Hutchinson, J.W., Wadley, H.N.G., 2000. Metal Foams: a Design Guide. Butterworth-Heinemann, Stoneham, MA.

Banhart, J., 2001. Manufacture, characterization and application of cellular metals and metal foams. Progress in Materials Science 46, 559–632.

Barber, C.B., Dobkin, D.P., Huhdanpaa, H.T., 1996. The Quickhull algorithm for convex hulls. ACM Transactions on Mathematical Software 22, 469–483.

Chen, C., Lu, T.J., Fleck, N.A., 1999. Effect of imperfections on the yielding of two dimensional foams. Journal of the Mechanics and Physics of Solids 47, 2235–2272.

Deshpande, V.S., Fleck, N.A., 2001. Multi-axial yield behavior of polymer foams. Acta Materialia 49, 1859–1866.
Gibson, L.J., Ashby, M.F., 1997. Cellular Solids: Structure and Properties. Cambridge University Press, Cambridge.
Gong, L., Kyriakides, S., Jang, W.-Y., 2005. Compressive response of open-cell foams. Part I: Morphology and elastic properties. International Journal of Solids and Structures 42, 1355–1379.
Gong, L., Kyriakides, S., 2005. Compressive response of open cell foams. Part II: Initiation and evolution of crushing. International Journal of Solids and Structures 42, 1381–1399.
Grenestedt, J.L., 1998. Influence of wavy imperfections in cell walls on elastic stiffness of cellular solids. Journal of the Mechanics and Physics of Solids 46, 29–50.
Gu, S., Lu, T.J., Evans, A.G., 2001. On the design of two-dimensional cellular metals for combined heat dissipation and structural load capacity. International Journal of Heat and Mass Transfer 44, 2163–2175.
Kraynik, A.M., Neilsen, M.K., Reinelt, D.A., Warren, W.E., 1997. Foam micromechanics. In: Proceedings of the NATO Advanced Study Institute on "Foams, Emulsions, and Cellular Materials", Cargese, Corsica.
Lu, T.J., Chen, C., 1999. Thermal transport and fire retardance properties of cellular aluminium alloys. Acta Materialia 47, 1469–1485.
Mahin, K.W., Hanson, K., Morris Jr., J.W., 1980. Comparative analysis of the cellular and Johnson–Mehl microstructures through computer simulation. Acta Metallugical 28, 443–453.
Okabe, A., Boots, B., Sugihara, K., Chiu, S., 2000. Spatial Tessellations, second ed. Wiley, Chichester.
Papka, S.D., Kyriakides, S., 1998a. In-plane crushing of a polycarbonate honeycomb. International Journal of Solids Structure 35, 239–267.
Papka, S.D., Kyriakides, S., 1998b. Experiments and full scale numerical simulations of in-plane crushing of a honeycomb. Acta Materialia 35, 2765–2776.
Roberts, A.P., Garboczi, E.J., 2001. Elastic moduli of model random three-dimensional closed-cell cellular solids. Acta Materialia 49, 189–197.
Roberts, A.P., Garboczi, E.J., 2002. Elastic properties of model random three-dimensional open-cell solids. Journal of the Mechanics and Physics of Solids 50, 33–55.
Shulmeister, V., Van der Burg, M.W.D., Van der Giessen, E., Marissen, R., 1998. A numerical study of large deformations of low-density elastomeric open-cell foams. Mechanics of Materials 30, 125–140.
Silva, M.J., Gibson, L.J., 1997. The effect of non-periodic microstructure and defects on the compressive strength of two-dimensional cellular solids. International Journal of Mechanical Sciences 39, 549–563.
Silva, M.J., Hayes, W.C., Gibson, L.J., 1995. The effects of non-periodic microstructure on the elastic properties of two-dimensional cellular solids. International Journal of Mechanical Sciences 11, 1161–1177.
Simone, A.E., Gibson, L.J., 1998. The effects of cell face curvature and corrugations on the stiffness and strength of metallic foams. Acta Materialia 46, 3929–3935.
Triantafyllidis, N., Schraad, M.W., 1998. Onset of failure in aluminum honeycombs under general in-plane loading. Journal of the Mechanics and Physics of Solids 46, 1089–1124.
Wang, Y., Cuitino, A.M., 2000. Three-dimensional nonlinear open-cell foams with large deformations. Journal of the Mechanics and Physics of Solids 48, 961–988.
Warren, W.E., Kraynik, A.M., 1987. Foam mechanics: the linear elastic response of two-dimensional spatially periodic cellular materials. Mechanics of Materials 6, 27–37.
Warren, W.E., Kraynik, A.M., 1991. The nonlinear elastic behavior of open-cell foams. ASME Journal of Applied Mechanics 58, 376–381.
Warren, W.E., Kraynik, A.M., 1997. Linear elastic behavior of a low-density Kelvin foam with open cells. ASME Journal of Applied Mechanics 64, 787–794.
Zhu, H.X., Mills, N.J., Knott, J.F., 1997. Analysis of the high strain compression of open-cell foams. Journal of the Mechanics and Physics of Solids 45, 1875–1904.
Zhu, H.X., Hobdell, J.R., Windle, A.H., 2000. Effects of cell irregularity on the elastic properties of open-cell foams. Acta Materialia 48, 4893–4900.
Zhu, H.X., Windle, A.H., 2002. Effects of cell irregularity on the high strain compression of open-cell foams. Acta Materialia 50, 1041–1052.